HOKKAIDO UNIVERSITY

Title	Comparison of skin barrier abnormalities and epidermal ceramide profiles among three ω-O-acylceramide synthesis-deficient mouse strains
Author(s)	Yamamoto, Yuta; Sassa, Takayuki; Kihara, Akio
Citation	Journal of dermatological science, 113(1), 10-17 https://doi.org/10.1016/j.jdermsci.2023.12.003
Issue Date	2024-01
Doc URL	https://hdl.handle.net/2115/94059
Rights	©2023. This manuscript version is made available under the CC-BY-NC-ND 4.0 license http://creativecommons.org/licenses/by-nc-nd/4.0/
Rights(URL)	https://creativecommons.org/licenses/by-nc-nd/4.0/
Type	journal article
File Information	Yamamoto et al.pdf

Hokkaido University Collection of Scholarly and Academic Papers : HUSCAP

Comparison of skin barrier abnormalities and epidermal ceramide profiles among three ω-*O*-acylceramide synthesis-deficient mouse strains

Yuta Yamamoto, Takayuki Sassa*, and Akio Kihara*

Laboratory of Biochemistry, Faculty of Pharmaceutical Sciences, Hokkaido University, Sapporo 060-0812, Japan

*Correspondence:

Takayuki Sassa and Akio Kihara

Laboratory of Biochemistry, Faculty of Pharmaceutical Sciences

Hokkaido University

Kita 12-jo, Nishi 6-chome, Kita-ku, Sapporo 060-0812, Japan

Tel: +81-11-706-3917 (T.S) and +81-11-706-3754 (A.K.)

Fax: +81-11-706-4900

E-mail: tasasa@pharm.hokudai.ac.jp (T.S) and kihara@pharm.hokudai.ac.jp (A.K.)

Funding sources

This work was supported by KAKENHI (grant numbers; JP22H04986 to A.K. and JP22H02757 to T.S.) from the Japan Society for the Promotion of Science (JSPS).

Conflicts of interest

The authors have no conflicts of interest to declare.

Text word count, 3471 words; number of references, 32; number of figures, 5; number of tables, 1; number of supplementary figures, 6.

Abstract

Background: The epidermis contains many structurally diverse ceramides, which form the skin permeability barrier (skin barrier). Mutations in genes involved in the synthesis of ω-*O*-acylceramides (acylceramides) and protein-bound ceramides cause ichthyosis.

Objective: We aimed to elucidate the relationship between the degree of skin barrier impairment and changes in epidermal ceramide profiles caused by mutations in acylceramide synthesis genes.

Methods: Knockout (KO) mice of three genes—fatty acid (FA) ω-hydroxylase *Cyp4f39* (human *CYP4F22* ortholog), FA elongase *Elovl1*, and acyl-CoA synthetase *Fatp4*—were subjected to transepidermal water loss measurement, toluidine blue staining, and epidermal ceramide profiling via liquid chromatography coupled with tandem mass spectrometry.

Results: Transepidermal water loss was highest in *Cyp4f39* KO mice, followed by *Elovl1* KO and *Fatp4* KO mice, and *Cyp4f39* KO mice also showed the strongest degree of toluidine blue staining. In *Cyp4f39* KO, *Elovl1* KO, and *Fatp4* KO mice, acylceramide levels were 0.6%, 1.6%, and 12%, respectively, of those in wild-type mice. Protein-bound ceramide levels were 0.2%, 30%, and 33%, respectively, of those in wild-type mice. We also observed a near-complete absence of ω-hydroxy ceramides in *Cyp4f39* KO mice, reduced total ceramide levels and shortened FA moieties in *Elovl1* KO mice, and increased hydroxylated ceramide levels and slightly shortened FA moieties in *Fatp4* KO mice.

Conclusions: The degree of reduction in protein-bound ceramide levels is probably related to the severity of skin barrier defects in these three strains. However, reduced acylceramide levels and other changes in ceramide composition unique to each KO strain are also involved.

Key words: Acylceramide, Ceramide, Knockout mouse, Mass spectrometry, Protein-bound ceramide, Skin permeability barrier

Abbreviations: A, α-hydroxy; acylceramide, ω-*O*-acylceramide; B, β-hydroxy; CLE, corneocyte lipid envelope; DS, dihydrosphingosine; EO, esterified ω-hydroxy; FA, fatty acid; H, 6-hydroxysphingosine; KO, knockout; LC, liquid chromatography; LCB, long-chain base; MS/MS, tandem mass spectrometry; N, nonhydroxy; O, ω-hydroxy; P, phytosphingosine; P-O, protein-bound ω-hydroxy; S, sphingosine; SC, stratum corneum; SD, 4,14-sphingadiene; TEWL, transepidermal water loss; WACL, weighted average chain length; WT, wild-type.

Running title: Comparison of acylceramide-deficient mouse strains

1. Introduction

The skin epidermis acts as a permeability barrier (hereafter referred to as the skin barrier) that prevents infection, invasion of allergens and chemicals, and loss of body fluid [1]. Reduction in skin barrier function causes or increases the risk of infectious disease, atopic dermatitis, dry skin, and ichthyosis. The stratum corneum (SC), the outermost layer of the epidermis, contains lipid lamellae and corneocyte lipid envelopes (CLEs), which are important for the formation and maintenance of the skin barrier [2,3]. The lipid lamellae are extracellular multilayered lipid structures composed of ceramides, cholesterol, and free fatty acids (FAs) [2,3], while CLEs are plasma membrane-like structures that cover corneocytes and are composed of protein-bound ceramides [4,5].

Ceramides consist of a long-chain base (LCB) and an FA linked by an amide bond [6]. In mammalian ceramides, there are five types of LCB (dihydrosphingosine [DS], sphingosine [S], phytosphingosine [P], 6-hydroxysphingosine [H], and 4,14-sphingadiene [SD]) and six types of FA (nonhydroxy FA [N], α-hydroxy FA [A], β-hydroxy FA [B], ω-hydroxy FA [O], esterified ω-hydroxy FA [EO], and protein-bound ω-hydroxy FA [P-O]) [6,7] (Fig. S1A). According to the types of the constituent LCB and FA moieties, ceramides are classified into 30 classes, which are named using abbreviations for the LCB and FA types (Fig. S1B). For example, NS ceramide consists of an N-type FA and an S-type LCB (Fig. S1C). The five classes of ceramides (EODS, EOS, EOP, EOH, and EOSD) that contain EO-type FAs, in which C18:2 linoleic acid (predominantly) is esterified to ω-hydroxy groups of O-type FAs, are called ω-*O*-acylceramides (acylceramides).

Of the 30 classes of ceramides, 25 are categorized as free ceramides (non-protein-bound ceramides); the remaining five classes, which are protein-bound ceramides that contain P-O-

type FAs, are excluded from this category. The FAs constituting ceramides are generally saturated or monounsaturated, but their chain lengths vary. The chain lengths are C16–C30 for N-, A-, and B-types, but C30–C36 for O-, EO-, and P-O-types [6,7]. We have previously reported the presence of 18 classes of free ceramides and five classes of protein-bound ceramides in human SC and the presence of 16 classes of free ceramides and four classes of protein-bound ceramides in mouse SC [7,8]. H- and B-type ceramides are found almost exclusively in humans and mice, respectively [7,8].

Acylceramides and protein-bound ceramides are present in a limited number of tissues, including the epidermis, oral mucosa, and esophagus [9-11]. In the epidermis, acylceramides play an important role in the formation of the lipid lamellae [3,12,13]. Protein-bound ceramides may protect corneocytes from external substances, including detergents, by binding tightly to the cells through covalent bonds, and they may ensure that the lipid lamellae remain stably on the corneocytes. All genes currently known to be involved in the synthesis of acylceramides or protein-bound ceramides are causative genes for congenital ichthyosis [14,15]. The acylceramide synthesis pathway includes the following reactions (Fig. S1D): (1) production of C30–C36 acyl-CoAs [16-18], (2) CoA removal, (3) ω-hydroxylation of C30–C36 FAs [19], (4) production of O-type C30–C36 acyl-CoAs [20], (5) synthesis of O-type ceramides [21], and (6) production of acylceramides via transacylation of linoleic acid from triacylglycerols to the O-type ceramides [22]. Protein-bound ceramides are synthesized from acylceramides via partially understood mechanisms that involve a series of modifications of the linoleic acid moiety [5,23,24].

Knockout (KO) mice lacking the genes mentioned above exhibit reduced levels of acylceramides and protein-bound ceramides, congenital ichthyosis-like skin phenotypes

including skin barrier impairment, and neonatal lethality [18,20,21,25-27]. However, the degree of reduction in the levels of acylceramides and protein-bound ceramides differs among the KO mouse strains, and it is unclear whether such differences are correlated with the degree of impairment of the skin barrier. Furthermore, only specific subsets of ceramide classes were analyzed in those KO mouse strains, so it is unclear whether the reductions in the levels of acylceramides and protein-bound ceramides induce any common or gene-specific compensatory changes in the ceramide profiles. It is also unclear whether such changes, if present, are associated with the skin barrier impairment.

We have recently established an analytical method involving the separation and quantification of ceramides by liquid chromatography coupled with tandem mass spectrometry (LC-MS/MS) [7]. In the present study, we applied this method to three mouse strains we had generated previously, each with one of the genes involved in the synthesis of acylceramides knocked out: *Cyp4f39* KO, *Elovl1* KO, and *Fatp4* KO [18,20,26]. We performed a comprehensive analysis of their epidermal ceramides and measured their skin barrier function under the same conditions and examined the relationship between the alterations in their ceramide profiles and the degree of skin barrier impairment.

2. Materials and methods

2.1 Mice

The *Cyp4f39* KO, *Elovl1* KO, and *Fatp4* KO mice used in this study were generated previously [18,20,26]. All animal experiments were approved by the institutional animal care and use committee of Hokkaido University. The KO mouse strains were maintained as heterozygous KO mice by repeated backcrossing with C57BL/6J mice. Newborn pups were obtained by Caesarean delivery at embryonic day 18.5 (E18.5). The homozygous KO and littermate wild-type (WT) mice were used for the experiments.

2.2 Skin permeability barrier assays

The transepidermal water loss (TEWL) was measured on the dorsal skin of E18.5 mice using an evaporimeter Vapo Scan AS-VT100RS (Asch Japan, Tokyo, Japan). After the TEWL measurement, mice were subjected to toluidine blue staining or the sampling of dorsal skin for lipid or RNA extraction. For the toluidine blue staining, mice were euthanized and immersed in methanol for 5 min, washed with PBS, and then incubated in 0.1% (w/v) toluidine blue in PBS at room temperature. The mice were retrieved from the staining solution after 30 min, 1 h, 2 h, and 24 h, washed with PBS, and photographed.

2.3 *Lipid extraction from the epidermis*

Dorsal skin dissected from E18.5 mice was incubated with 5 mg/mL dispase (Thermo Fisher Scientific, Waltham, MA, USA) in PBS for 16 h at 4 °C, after which the epidermis was separated from the dermis. The lipids were extracted from the epidermis, as described in detail in the Supplementary Materials and Methods.

2.4 *LC-MS/MS analysis of ceramides*

Free ceramides and protein-bound ceramides were subjected to LC-MS/MS analysis using an LC-coupled triple quadrupole mass spectrometer (Xevo TQ-S; Waters, Milford, MA, USA) as described previously [7].

2.5 *Quantitative RT-PCR*

Dorsal skin dissected from E18.5 mice was incubated in PBS for 3 min at 55 °C, and the epidermis was separated from the dermis. Total RNA was isolated from the epidermis using TRIzol Reagent (Thermo Fisher Scientific) and converted to first-strand cDNA using oligo dT primers and the PrimeScript II 1st Strand cDNA Synthesis Kit (Takara Bio, Shiga, Japan), according to the manufacturer's instructions. Real-time quantitative PCR was performed using the first-strand cDNA, primer pairs specific to each gene (Degs1-F/-R, Degs2-F/-R, and Hprt-F/-R; Table 1), and KOD SYBR qPCR Mix (Toyobo, Osaka, Japan) on the CFX96 Touch real-time PCR detection system (Bio-Rad, Hercules, CA, USA). The mRNA level of each gene was normalized with respect to *Hprt*.

3. Results

3.1 Different degrees of skin barrier impairment in Cyp4f39 KO, Elovl1 KO, and Fatp4 KO mice

We have previously reported that the FA ω-hydroxylase *Cyp4f39* (human *CYP4F22* ortholog), the FA elongase *Elovl1*, and the acyl-CoA synthetase *Fatp4* are involved in the synthesis of acylceramides, and KO mice for each gene exhibit impairments in skin barrier formation and neonatal lethality [18–20,26]. In this study, we compared the degree of impairment in skin barrier formation among these three KO mouse strains. We examined the permeability barrier function from outside the body via toluidine blue staining. After 30 min of staining, the *Cyp4f39* KO mice were strongly stained throughout the body, whereas the staining of the *Elovl1* KO and *Fatp4* KO mice was weaker and partial (Fig. 1A). In *Cyp4f39* KO mice, the staining was already saturated at 30 min and did not differ noticeably from staining for longer durations (1, 2, and 24 h). In contrast, the staining of *Elovl1* KO and *Fatp4* KO mice became more extensive and stronger as the staining period was prolonged, such that the entire body was stained at 24 h. The degree of staining at 24 h was strongest in *Cyp4f39* KO mice, followed by that in *Elovl1* KO and *Fatp4* KO mice, which displayed similar degrees of staining.

We measured TEWL to evaluate the permeability barrier from inside the body. All KO mouse strains exhibited significantly higher TEWL values than WT mice (Fig. 1B). The TEWL values were the highest in *Cyp4f39* KO mice, followed by those in *Elovl1* KO and *Fatp4* KO mice. These results indicated that the *Cyp4f39* KO mice exhibited by far the most severe skin barrier impairment among the three strains, and the *Elovl1* KO mice exhibited slightly more severe impairment than the *Fatp4* KO mice.

3.2 Different degrees of reduction in acylceramide and protein-bound ceramide levels in Cyp4f39 KO, Elovl1 KO, and Fatp4 KO mice

To compare the ceramide composition of the epidermis of *Cyp4f39* KO, *Elovl1* KO, and *Fatp4* KO mice, we subjected their epidermal lipids to LC-MS/MS. In WT mice, the acylceramides EOS, EODS, EOP, and EOSD were present, with EOS accounting for approximately 90% of total acylceramides (Fig. 2A–C). The total acylceramide levels in *Cyp4f39* KO, *Elovl1* KO, and *Fatp4* KO mice were 0.6%, 1.6%, and 12%, respectively, of those in WT mice. All four acylceramide classes were reduced, except for EOP in *Fatp4* KO mice (Fig. 2C). Each acylceramide class includes several molecular species with different chain lengths (C30–C36) and degrees of unsaturation (saturated or monounsaturated) in the ω-hydroxy FA portion. All EOS species were reduced in *Cyp4f39* KO, *Elovl1* KO, and *Fatp4* KO mice relative to WT mice (Fig. 2D–F).

In WT mice, P-OS accounted for ≥ 95% of total protein-bound ceramide levels (Fig. 3A–C). The total protein-bound ceramide levels in *Cyp4f39* KO, *Elovl1* KO, and *Fatp4* KO mice were 0.2%, 30%, and 33%, respectively, of those in WT mice. Although the quantities of most protein-bound ceramide classes were reduced in these KO mice relative to WT mice, P-OP levels in *Fatp4* KO mice were substantially increased (Fig. 3C). In *Cyp4f39* KO mice, all P-OS species were almost entirely absent (Fig. 3D). In *Elovl1* KO and *Fatp4* KO mice, P-OS species with a saturated ω-hydroxy FA moiety were greatly reduced, but those with a monounsaturated ω-hydroxy FA moiety were only slightly reduced (Fig. 3D–F). In summary, the degrees of reduction in acylceramide and protein-bound ceramide levels varied among the three KO mouse strains, with the order of severity as follows: *Cyp4f39* KO, *Elovl1* KO, *Fatp4* KO.

In these KO mouse strains, we also observed compositional changes in free ceramides other than acylceramides (Fig. 4A). In *Cyp4f39* KO mice, the levels of O-type ceramides (OS, ODS, OP, and OSD) and ASD were substantially reduced (O-type ceramides, ~5%; ASD, 65% of those in WT mice), whereas those of NDS, NS, and BS were increased (although the increases in NS and BS were not statistically significant). Total free ceramide levels were similar in *Cyp4f39* KO and WT mice. In *Elovl1* KO mice, O-type ceramide levels were severely reduced, as they were in *Cyp4f39* KO mice. Levels of NS, NDS, NSD, AS, ASD, and BS were also substantially reduced. Total free ceramide levels were ~25% of WT mice. In *Fatp4* KO mice, levels of NDS, OS, and ODS were reduced, whereas those of NP, NSD, AS, BS, and OP were increased. Of these, levels of NP and OP were increased 8.4-fold and 9.0-fold, respectively, relative to WT mice. Total free ceramide levels were comparable between *Fatp4* KO and WT mice.

With respect to FA composition, in *Cyp4f39* KO mice the reductions in the ceramides with O-type FAs (O-type ceramides) and EO-type FAs (acylceramides, EO-type) were compensated by the increases in N-type and B-type ceramides (Fig. 4B). In *Elovl1* KO mice, the proportions of O- and EO-type ceramides were greatly reduced, while those of A- and B-type ceramides were increased. In *Fatp4* KO mice, only the proportion of EO-type ceramides was substantially reduced, concomitant with the increased proportions of A- and B-type ceramides.

The LCB composition did not change noticeably in *Cyp4f39* KO or *Elovl1* KO mice relative to WT mice (Fig. 4C). In contrast, the proportions of P-type and DS-type ceramides were increased and decreased, respectively, in *Fatp4* KO mice (Fig. 4C), which reflected the increase in NP and decrease in NDS levels in these mice (Fig. 4A).

The FA chain lengths of N-, A-, and B-type ceramides are C16–C30 [7]. In WT mice, N-type ceramides (NS, NDS, and NP) predominantly comprised C26:0 FA, followed by C24:0 FA (Figs. S2–S4). In contrast, the most abundant FA species in AS was C16:0 (Fig. S5) and in BS were C26:0 and C28:0 (Fig. S6). The weighted average chain lengths (WACL) of the FA moieties of NS, NDS, NP, AS, and BS increased in *Cyp4f39* KO mice relative to WT mice (Fig. 4D). In contrast, the WACLs of all five classes decreased in *Elovl1* KO and *Fatp4* KO mice. In particular, *Elovl1* KO mice exhibited substantially reduced WACLs (difference from WT mice: 0.78–3.03).

3.3 Increased expression levels of the dihydroceramide hydroxylase Degs2 in Fatp4 KO mice

Fatp4 KO mice appeared to exhibit complementary changes in their ceramide class composition: increases in NP and OP and decreases in NDS and ODS (Fig. 4A). NP and OP are respectively synthesized from the DS-type ceramides (dihydroceramides) NDS and ODS via the 4-hydroxylation of the DS-portion, suggesting that the conversion of ceramides from DS-type to P-type is enhanced in the epidermis of *Fatp4* KO mice. Therefore, we next examined the expression levels of the dihydroceramide 4-hydroxylase *Degs2* in the epidermis of *Cyp4f39* KO, *Elovl1* KO, and *Fatp4* KO mice using quantitative RT-PCR. The *Degs2* mRNA levels in *Fatp4* KO mice were 12-fold those in WT mice, but no such increase was observed in *Cyp4f39* KO or *Elovl1* KO mice (Fig. 5A). We also examined the expression levels of the dihydroceramide 4-desaturase *Degs1*, which converts DS-type ceramides to S-type ceramides. The *Degs1* mRNA levels were 1.7-fold and 1.8-fold those in WT mice in *Elovl1* KO and *Fatp4* KO mice, respectively (Fig. 5B). Thus, the increase in *Degs2* expression levels was mainly

responsible for the increases in P-type ceramides and decreases in DS-type ceramides in *Fatp4* KO mice.

4. Discussion

Analyses of the skin barrier in three KO mouse strains of acylceramide synthesis genes revealed that *Cyp4f39* KO mice exhibited much more severe skin barrier impairment than *Elovl1* KO or *Fatp4* KO mice (Fig. 1). This severe phenotype of *Cyp4f39* KO can be explained by the near-complete absence of both acylceramides (0.6% of WT mice) and protein-bound ceramides (0.2% of WT mice) (Figs. 2 and 3). In *Elovl1* KO mice, acylceramides were greatly reduced (1.6 % of WT mice), whereas protein-bound ceramides were only reduced to 30%. Thus, the milder impairment of the skin barrier in *Elovl1* KO mice than in *Cyp4f39* KO mice is mainly accounted for by the residual protein-bound ceramides. In *Fatp4* KO mice, the degree of reduction in protein-bound ceramide levels was similar to that in *Elovl1* KO mice, but the acylceramide levels were higher in *Fatp4* KO than *Elovl1* KO mice. This difference in acylceramide levels may thus at least partially account for the milder skin barrier impairment in *Fatp4* KO mice than in *Elovl1* KO mice (Fig. 1B).

The three KO mouse strains did not show common composition changes in any free ceramides other than acylceramides, but instead characteristic changes were observed in each strain. In *Cyp4f39* KO mice, levels of ceramide species with a C32–C36 FA moiety were increased in some classes, such as NS, NDS, and BS (Figs. S2, S3, and S6), and their WACLs were increased relative to WT mice (Fig. 4D). These changes resulted from the deficiency in *Cyp4f39* KO mice in ω-hydroxylation of C32–C36 FAs, which are substrates of Cyp4f39 and are converted to O-type C32–C36 FAs by it. Instead, these FAs were incorporated into other types of ceramides.

In *Elovl1* KO mice, total ceramide levels were reduced to about 25% of those in WT mice for unknown reasons (Fig. 4A). In congenital ichthyosis patients with a recessive homozygous

mutation in the *ELOVL1* gene, their acylceramide levels were reduced, similarly to the *Elovl1* KO mice in this study, but their total ceramide levels were almost unchanged [28]. Thus, a reduction in total ceramide levels caused by a mutation in *Elovl1* appears to be unique to mice. Considering that total ceramide levels did not change in *Cyp4f39* KO and *Fatp4* KO mice, which exhibited more severe and milder skin barrier impairment, respectively (Fig. 1), than *Elovl1* KO mice (Fig. 4A), the marked reduction in total ceramide levels in *Elovl1* KO mice may have little, if any, effect on skin barrier function. *Elovl1* KO mice exhibited shortening of the FA moiety in most ceramide classes, since the FA elongase ELOVL1 is involved in the elongation of C20–C24 acyl-CoAs to C24–C26 acyl-CoAs [17,18].

In *Fatp4* KO mice, NP, AS, BS, and OP were increased and NDS and ODS were reduced relative to WT mice (Fig. 4A). The increased ceramide classes have one more hydroxyl group than NS, which is the most abundant ceramide class in mouse epidermis, and they can stabilize the lipid lamellae by enhancing lipid–lipid interactions via hydrogen bonds and improve skin barrier function. These increases may have arisen from compensatory responses to restore the reduced skin barrier function resulting from the *Fatp4* deficiency. One noticeable response was the increased expression of *Degs2* (Fig. 5), which may have contributed to the increases in NP and OP and decreases in NDS and ODS. *Fatp4* KO mice also exhibited slight shortening of the FA moiety (Fig. 4D, Figs. S2–6). Based on the previous expression analyses of genes involved in the synthesis of ceramides in the three KO mouse strains [18,20,26], the shortening of the FA moiety in *Fatp4* KO mice is probably due to reduced expression of *Elovl1* [20], although the causal mechanism for this reduction is unknown. The expression levels of *Pnpla1* are also reduced in *Fatp4* KO mice [20], which may partly contribute to the decrease in acylceramide levels. All these differences in the ceramide composition and FA chain lengths, together with

changes in acylceramide levels, may account for the differences in the degree of skin barrier defects between *Elovl1* KO and *Fatp4* KO mice.

Acyl-CoAs are elongated by the FA elongation cycle, which consists of four sequential steps: condensation, reduction, dehydration, and reduction [29,30]. In the rate-limiting condensation reaction, an acyl-CoA (*n*), where *n* indicates the number of carbons, is condensed with malonyl-CoA, resulting in the production of β-ketoacyl-CoA (*n* + 2). The β-ketoacyl-CoA (*n* + 2) is reduced to β-hydroxyacyl-CoA (*n* + 2), then dehydrated to *trans*-2-enoyl-CoA (*n* + 2), and finally reduced to acyl-CoA (*n* + 2). The acyl-CoA is thus elongated by two carbons per cycle.

In mammals, the first condensation reaction is catalyzed by seven fatty acid elongases (ELOVL1–7) and the third dehydration reaction is catalyzed by two β-OH acyl-CoA dehydratases (HACD1 and 2) [31,32]. We have previously proposed that β-hydroxyacyl-CoAs produced via the FA elongation cycle are used for B-type ceramide synthesis, based on an analysis using *HACD1 HACD2* double KO cells, which accumulate β-hydroxyacyl-CoAs [7]. In this study, the most abundant FA moieties in the BS in WT mice were C26:0 and C28:0 (Fig. S6), which are two carbons longer than the major FA moieties C24:0 and C26:0 in NS (Fig. S2). In *Elovl1* KO mice, the major FA moieties in BS were C26:0 and C24:0, and the WACL of this BS was shortened by almost two carbons (Figs. 4 and S6). These results are consistent with our previous proposal that the FA moieties of B-type ceramides are generated via the FA elongation cycle.

In terms of skin morphology, all three KO mouse lines exhibited impaired lipid lamella formation in the hematoxylin-eosin stained sections [18,20,26]. In addition, *Cyp4f39* KO and *Fatp4* KO mice, but not *Elovl1* KO mice, showed hyperkeratosis. This difference may be

related to the reduction in total ceramide levels observed only in *Elovl1* KO mice among the three KO mouse strains. A limitation of this study is that it remains unknown how the changes in ceramide profiles cause the differences in the number of SC layers and in the expression of certain genes, such as *Degs2* and *Elovl1*.

In this study, we performed a comprehensive analysis of epidermal ceramides in three KO mouse strains with defective acylceramide production and found different changes in their ceramide profiles. These alterations may have contributed to the varying degrees of skin barrier abnormalities we observed in these mice. Our findings may be helpful for improving our understanding of pathological conditions associated with impaired skin barrier formation, such as atopic dermatitis and ichthyosis.

References

[1] E. Proksch, J.M. Brandner, J.M. Jensen, The skin: an indispensable barrier, Exp. Dermatol. 17 (2008) 1063–1072.

[2] K.R. Feingold, P.M. Elias, Role of lipids in the formation and maintenance of the cutaneous permeability barrier, Biochim. Biophys. Acta 1841 (2014) 280–294.

[3] J. van Smeden, M. Janssens, G.S. Gooris, J.A. Bouwstra, The important role of stratum corneum lipids for the cutaneous barrier function, Biochim. Biophys. Acta 1841 (2014) 295–313.

[4] P.M. Elias, R. Gruber, D. Crumrine, G. Menon, M.L. Williams, J.S. Wakefield, et al., Formation and functions of the corneocyte lipid envelope (CLE), Biochim. Biophys. Acta 1841 (2014) 314–318.

[5] T. Takeichi, T. Hirabayashi, Y. Miyasaka, A. Kawamoto, Y. Okuno, S. Taguchi, et al., SDR9C7 catalyzes critical dehydrogenation of acylceramides for skin barrier formation, J. Clin. Invest. 130 (2020) 890–903.

[6] A. Kihara, Synthesis and degradation pathways, functions, and pathology of ceramides and epidermal acylceramides, Prog. Lipid Res. 63 (2016) 50–69.

[7] M. Kawana, M. Miyamoto, Y. Ohno, A. Kihara, Comparative profiling and comprehensive quantification of stratum corneum ceramides in humans and mice by LC/MS/MS, J. Lipid Res. 61 (2020) 884–895.

[8] M. Suzuki, Y. Ohno, A. Kihara, Whole picture of human stratum corneum ceramides, including the chain-length diversity of long-chain bases, J. Lipid Res. 63 (2022) 100235.

[9] F. Chang, D.C. Swartzendruber, P.W. Wertz, C.A. Squier, Covalently bound lipids in keratinizing epithelia, Biochim. Biophys. Acta 1150 (1993) 98–102.

[10] T. Sassa, A. Kihara, Involvement of ω-*O*-acylceramides and protein-bound ceramides in oral permeability barrier formation, Cell Rep. 42 (2023) 112363.

[11] P.W. Wertz, M. Kremer, C.A. Squier, Comparison of lipids from epidermal and palatal stratum corneum, J. Invest. Dermatol. 98 (1992) 375–378.

[12] B. Breiden, K. Sandhoff, The role of sphingolipid metabolism in cutaneous permeability barrier formation, Biochim. Biophys. Acta 1841 (2014) 441–452.

[13] Y. Uchida, W.M. Holleran, Omega-*O*-acylceramide, a lipid essential for mammalian survival, J. Dermatol. Sci. 51 (2008) 77–87.

[14] M. Akiyama, Acylceramide is a key player in skin barrier function: insight into the molecular mechanisms of skin barrier formation and ichthyosis pathogenesis, FEBS J. 288 (2021) 2119–2130.

[15] J. Fischer, E. Bourrat, Genetics of Inherited Ichthyoses and Related Diseases, Acta. Derm. Venereol. 100 (2020) 186–196.

[16] Y. Mizutani, H. Sun, Y. Ohno, T. Sassa, T. Wakashima, M. Obara, et al., Cooperative synthesis of ultra long-chain fatty acid and ceramide during keratinocyte differentiation, PLoS One 8 (2013) e67317.

[17] Y. Ohno, S. Suto, M. Yamanaka, Y. Mizutani, S. Mitsutake, Y. Igarashi, et al., ELOVL1 production of C24 acyl-CoAs is linked to C24 sphingolipid synthesis, Proc. Natl. Acad. Sci. USA 107 (2010) 18439–18444.

[18] T. Sassa, Y. Ohno, S. Suzuki, T. Nomura, C. Nishioka, T. Kashiwagi, et al., Impaired epidermal permeability barrier in mice lacking *Elovl1*, the gene responsible for very-long-chain fatty acid production, Mol. Cell. Biol. 33 (2013) 2787–2796.

[19] Y. Ohno, S. Nakamichi, A. Ohkuni, N. Kamiyama, A. Naoe, H. Tsujimura, et al., Essential

role of the cytochrome P450 CYP4F22 in the production of acylceramide, the key lipid for skin permeability barrier formation, Proc. Natl. Acad. Sci. USA 112 (2015) 7707–7712.

[20] H. Yamamoto, M. Hattori, W. Chamulitrat, Y. Ohno, A. Kihara, Skin permeability barrier formation by the ichthyosis-causative gene FATP4 through formation of the barrier lipid ω-*O*-acylceramide, Proc. Natl. Acad. Sci. USA 117 (2020) 2914–2922.

[21] R. Jennemann, M. Rabionet, K. Gorgas, S. Epstein, A. Dalpke, U. Rothermel, et al., Loss of ceramide synthase 3 causes lethal skin barrier disruption, Hum. Mol. Genet. 21 (2012) 586–608.

[22] Y. Ohno, N. Kamiyama, S. Nakamichi, A. Kihara, PNPLA1 is a transacylase essential for the generation of the skin barrier lipid ω-*O*-acylceramide, Nat. Commun. 8 (2017) 14610.

[23] A. Muñoz-Garcia, C.P. Thomas, D.S. Keeney, Y. Zheng, A.R. Brash, The importance of the lipoxygenase-hepoxilin pathway in the mammalian epidermal barrier, Biochim. Biophys. Acta 1841 (2014) 401–408.

[24] Z. Nemes, L.N. Marekov, L. Fésüs, P.M. Steinert, A novel function for transglutaminase 1: attachment of long-chain omega-hydroxyceramides to involucrin by ester bond formation, Proc Natl Acad Sci U S A 96(15) (1999) 8402–8407.

[25] T. Hirabayashi, T. Anjo, A. Kaneko, Y. Senoo, A. Shibata, H. Takama, et al., PNPLA1 has a crucial role in skin barrier function by directing acylceramide biosynthesis, Nat. Commun. 8 (2017) 14609.

[26] M. Miyamoto, N. Itoh, M. Sawai, T. Sassa, A. Kihara, Severe skin permeability barrier dysfunction in knockout mice deficient in a fatty acid ω-hydroxylase crucial to acylceramide production, J. Invest. Dermatol. 140 (2020) 319–326.

[27] V. Vasireddy, Y. Uchida, N. Salem, Jr., S.Y. Kim, M.N. Mandal, G.B. Reddy, et al., Loss

of functional ELOVL4 depletes very long-chain fatty acids (≥C28) and the unique ω-O-acylceramides in skin leading to neonatal death, Hum. Mol. Genet. 16 (2007) 471–482.

[28] T. Takahashi, S. Mercan, T. Sassa, G.B. Akçapınar, K. Yararbaş, S. Süsgün, et al., Hypomyelinating spastic dyskinesia and ichthyosis caused by a homozygous splice site mutation leading to exon skipping in *ELOVL1*, Brain Dev. 44 (2022) 391–400.

[29] A. Kihara, Very long-chain fatty acids: elongation, physiology and related disorders, J. Biochem. 152 (2012) 387–395.

[30] T. Sassa, A. Kihara, Metabolism of very long-chain fatty acids: genes and pathophysiology, Biomol. Ther. 22 (2014) 83–92.

[31] M. Ikeda, Y. Kanao, M. Yamanaka, H. Sakuraba, Y. Mizutani, Y. Igarashi, et al., Characterization of four mammalian 3-hydroxyacyl-CoA dehydratases involved in very long-chain fatty acid synthesis, FEBS Lett 582(16) (2008) 2435–2440.

[32] M. Sawai, Y. Uchida, Y. Ohno, M. Miyamoto, C. Nishioka, S. Itohara, et al., The 3-hydroxyacyl-CoA dehydratases HACD1 and HACD2 exhibit functional redundancy and are active in a wide range of fatty acid elongation pathways, J Biol Chem 292(37) (2017) 15538–15551.

Figure legends

Fig. 1. Skin barrier impairment in *Cyp4f39* KO, *Elovl1* KO, and *Fatp4* KO mice. E18.5 pups of *Cyp4f39* KO (n = 4), *Elovl1* KO (n = 6), and *Fatp4* KO (n = 3) mice and their corresponding control WT mice (*Cyp4f39*, n = 13; *Elovl1*, n = 14; *Fatp4*, n = 7) were obtained via Caesarean delivery. (A) Mice were not stained or incubated with 0.1% toluidine blue for 30 min, 1 h, 2 h, and 24 h, washed with PBS, and photographed. (B) Measurement of TEWL. Values presented are means + SD, and statistically significant differences are indicated (** $P < 0.01$; Tukey–Kramer test).

Fig. 2. Acylceramide levels in *Cyp4f39* KO, *Elovl1* KO, and *Fatp4* KO mice. Lipids were extracted from the epidermis of E18.5 *Cyp4f39* KO (n = 3), *Elovl1* KO (n = 3), and *Fatp4* KO (n = 3) mice and their corresponding control WT mice (n =3 each), and acylceramides were analyzed via LC-MS/MS. (A–C) The quantity of each acylceramide class (left and middle panels) and the total of all classes (right panel). (D–F) The quantity of each EOS species containing the indicated O-type FA moiety (left panel) and the total quantities of saturated (S) species, monounsaturated (MU) species, and both (right panel). Values presented are means + SD, and statistically significant differences from WT mice are indicated (* $P < 0.05$, ** $P < 0.01$; Student's *t*-test).

Fig. 3. Protein-bound ceramide levels in *Cyp4f39* KO, *Elovl1* KO, and *Fatp4* KO mice. Epidermis was collected from E18.5 *Cyp4f39* KO (n = 3), *Elovl1* KO (n = 3), and *Fatp4* KO (n = 3) mice and their corresponding control WT mice (n =3 each). After free lipids had been removed from the epidermis, protein-bound ceramides were released as O-type ceramides via

alkaline treatment. The resulting O-type ceramides were extracted and subjected to LC-MS/MS analysis. (A–C) The quantity of each protein-bound ceramide class (left and middle panels) and the total of all classes (right panel). (D–F) The quantity of each P-OS species containing the indicated O-type FA moiety (left panel) and the total quantities of saturated (S) species, monounsaturated (MU) species, and both (right panel). Values presented are means + SD, and statistically significant differences from WT mice are indicated (* $P < 0.05$, ** $P < 0.01$; Student's *t*-test).

Fig. 4. Free-ceramide profiles for *Cyp4f39* KO, *Elovl1* KO, and *Fatp4* KO mice. Lipids were extracted from the epidermis of E18.5 *Cyp4f39* KO (n = 3), *Elovl1* KO (n = 3), and *Fatp4* KO (n = 3) mice and their corresponding control WT mice (n =3 each), and free ceramides were analyzed via LC-MS/MS. (A) The quantity of each ceramide class (left panels) and the total of all classes (right panels). (B) The composition of FA-types. (C) The composition of LCB-types. (D) Differences in the weighted average chain lengths (ΔCL) of NS, NDS, NP, AS, and BS classes in *Cyp4f39* KO, *Elovl1* KO, and *Fatp4* KO mice from those in WT mice. Values presented are means + SD, and statistically significant differences from WT mice are indicated (* $P < 0.05$, ** $P < 0.01$; Student's *t*-test).

Fig. 5. The mRNA levels of dihydroceramide 4-hydroxylase *Degs1* and dihydroceramide 4-desaturase *Degs2*. Total RNAs were extracted from the epidermis of E18.5 *Cyp4f39* KO (n =3), *Elovl1* KO (n = 3), and *Fatp4* KO (n = 3) mice and their corresponding control WT mice (n = 3 each), and the mRNA levels of *Degs2* (A) and *Degs1* (B) were analyzed via quantitative RT-PCR. Values presented are means + SD of each mRNA relative to that of the housekeeping

gene *Hprt*. Statistically significant differences from WT mice are indicated (* $P < 0.05$, ** $P < 0.01$; Student's *t*-test).

Table 1. List of oligonucleotide primers used for quantitative RT-PCR analysis

Oligonucleotide name	Sequence
Degs1-F	5′-GCCGAACATTACATGTTCTTGAAGG-3′
Degs1-R	5′-GTTCCCTTTCGGAGGCCTCTTCATC-3′
Degs2-F	5′-GTTCCTGAAGGGCCACGAGACTTAC-3′
Degs2-R	5′-GTGGTCCTTCGCCAGCTTACACTTG-3′
Hprt-F	5′-GCTGACCTGCTGGATTACATTAAAG-3′
Hprt-R	5′-CTTAACCATTTTGGGGCTGTACTGC-3′

Fig. 1

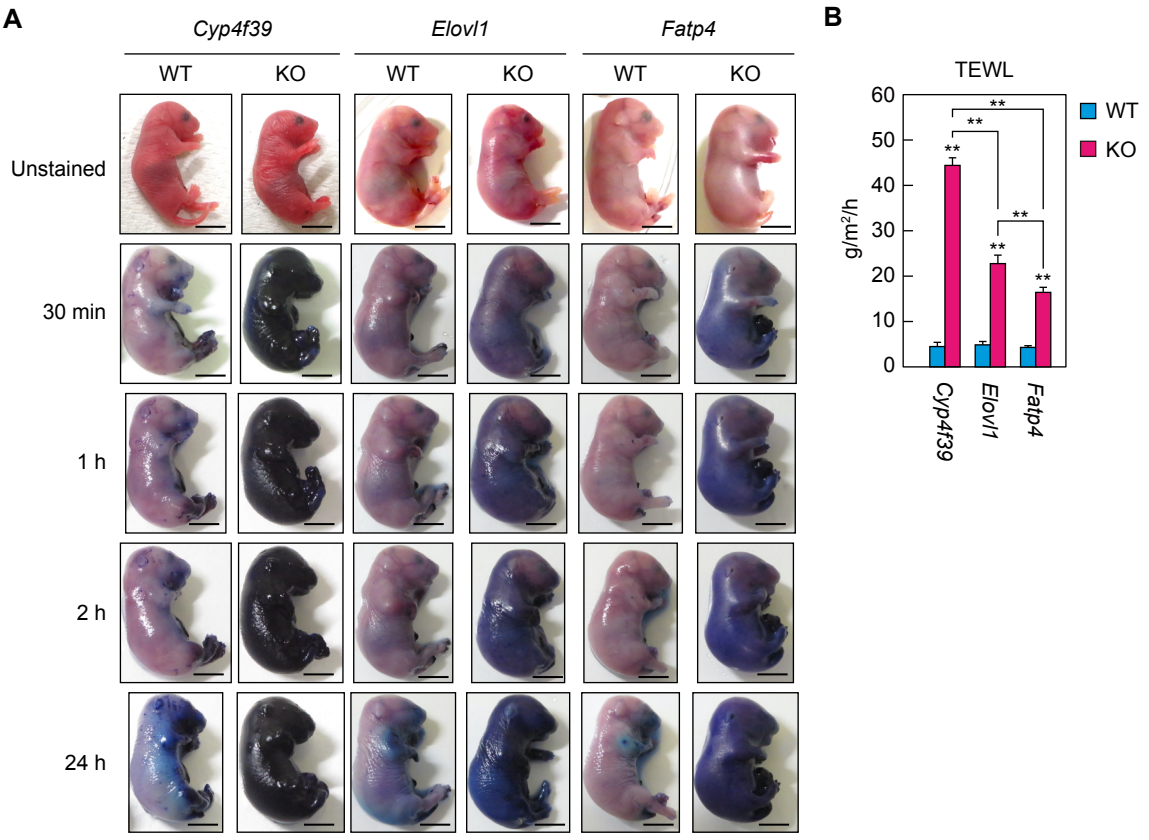

A
Cyp4f39
Elovl1
Fatp4
WT
KO
WT
KO
WT
KO
Unstained
30 min
1 h
2 h
24 h
B
TEWL
g/m²/h
60
50
40
30
20
10
0
**
**
**
**
**
**
WT
KO
Cyp4f39
Elovl1
Fatp4

Fig. 2

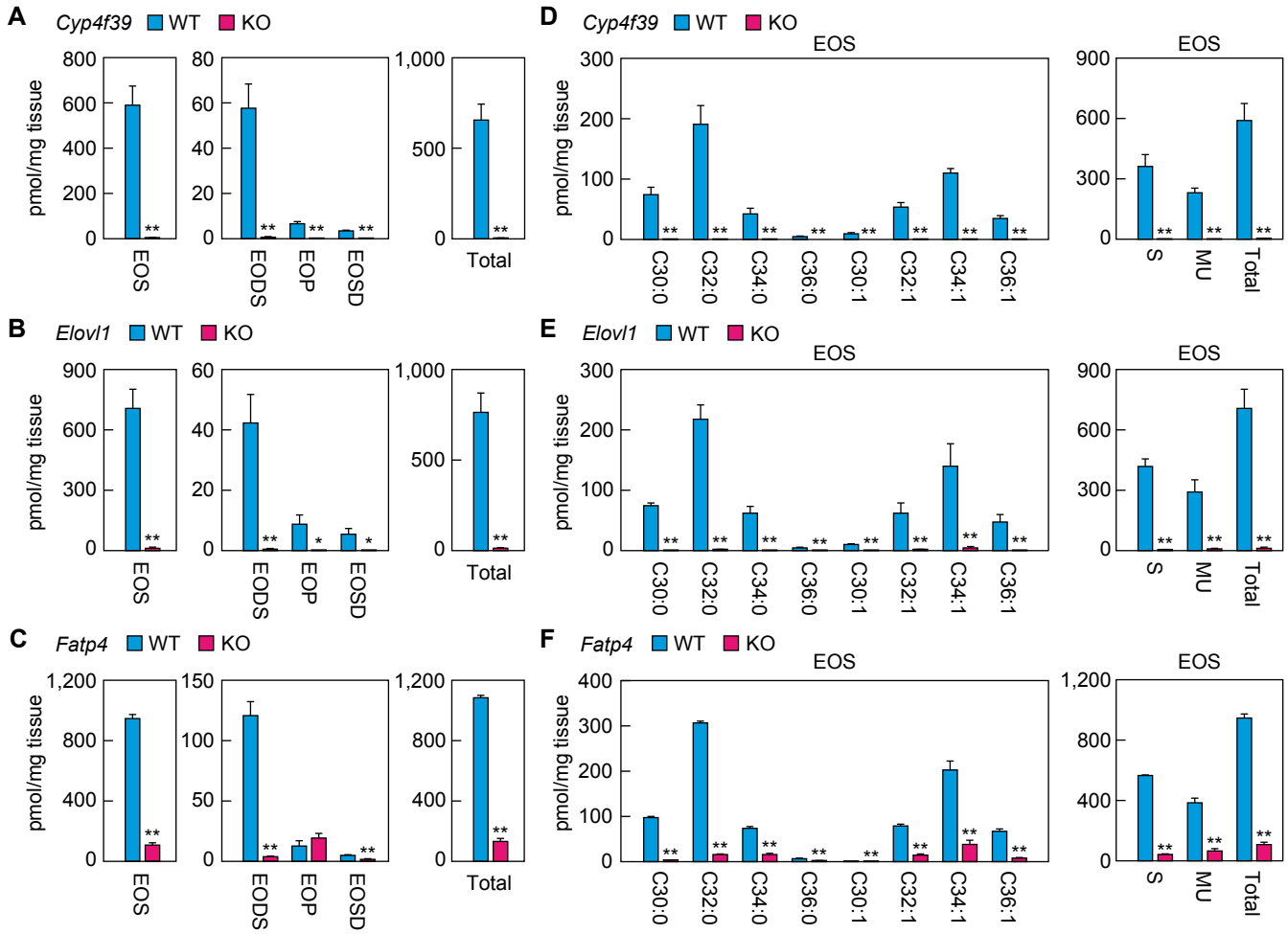

A
Cyp4f39 WT KO
pmol/mg tissue
EOS
EODS
EOP
EOSD
Total
B
Elovl1 WT KO
C
Fatp4 WT KO
D
Cyp4f39 WT KO
EOS
C30:0
C32:0
C34:0
C36:0
C30:1
C32:1
C34:1
C36:1
S
MU
Total
E
Elovl1 WT KO
F
Fatp4 WT KO

Fig. 3

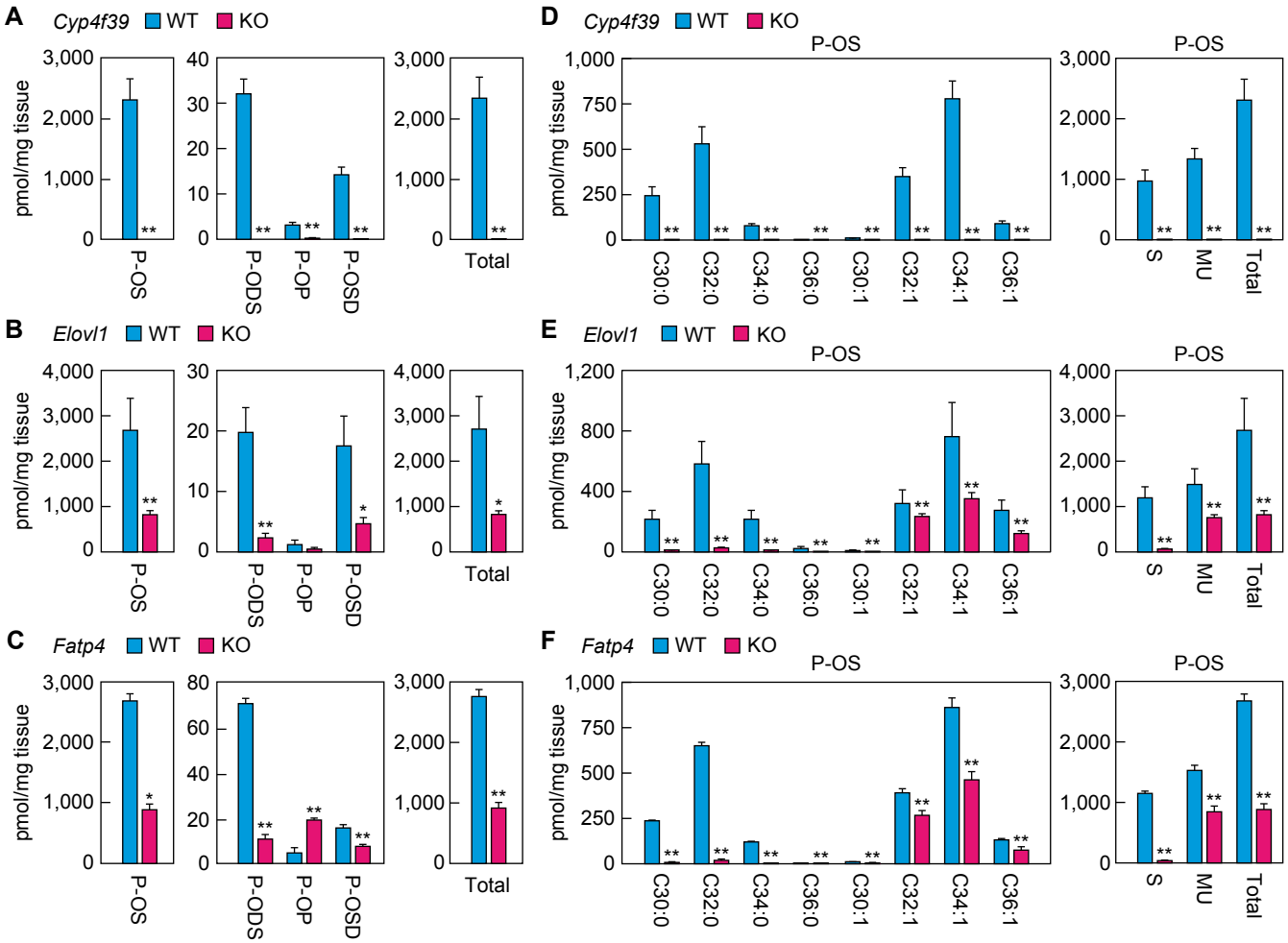

A
Cyp4f39 WT KO
pmol/mg tissue
P-OS
P-ODS
P-OP
P-OSD
Total
B
Elovl1 WT KO
C
Fatp4 WT KO
D
Cyp4f39 WT KO
P-OS
C30:0
C32:0
C34:0
C36:0
C30:1
C32:1
C34:1
C36:1
S
MU
Total
E
Elovl1 WT KO
F
Fatp4 WT KO

Fig. 4

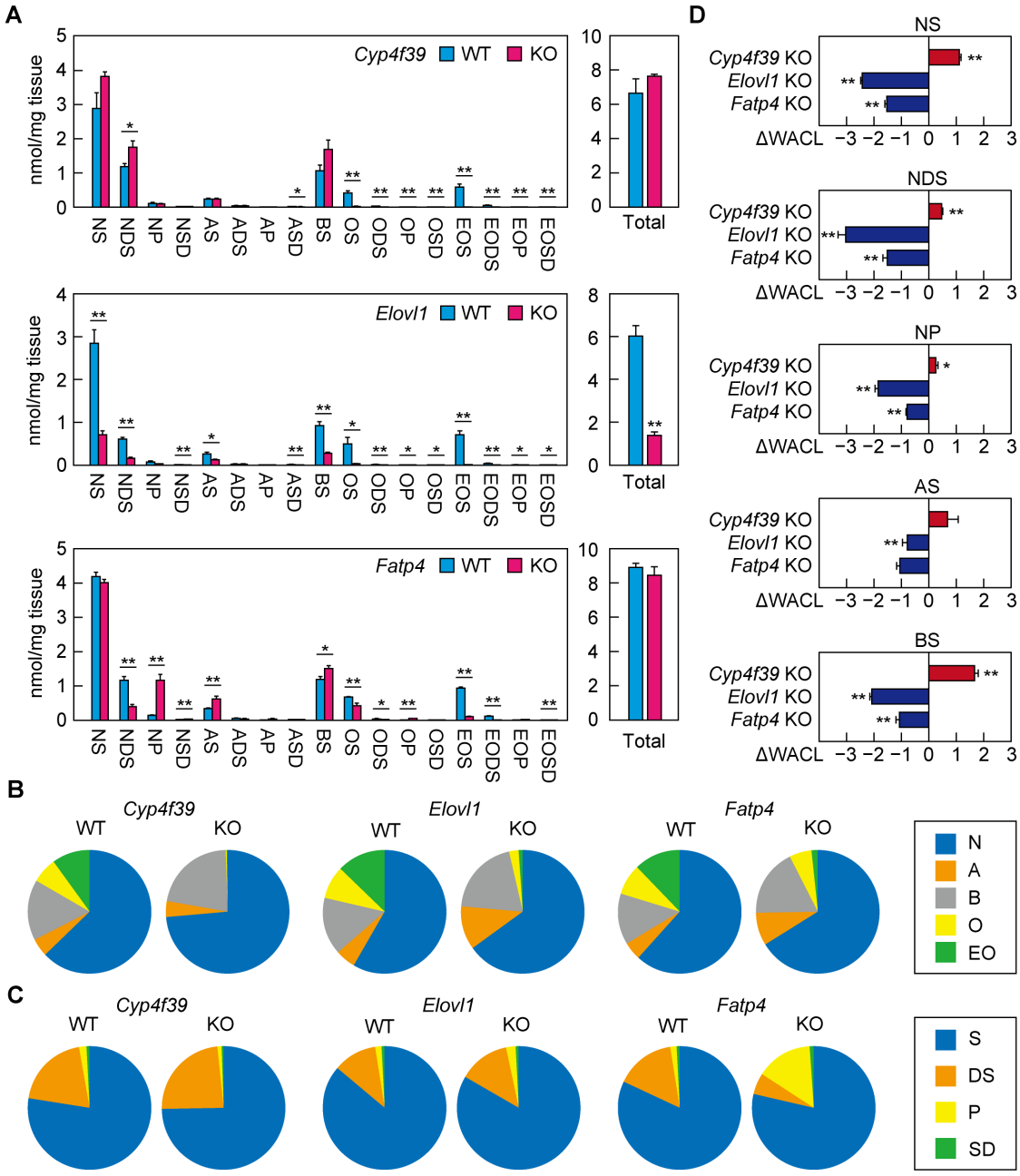
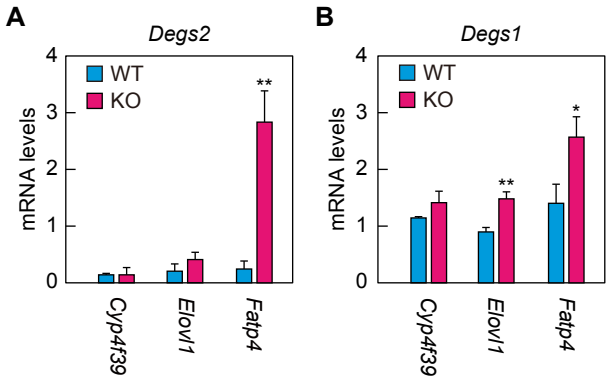

A
Cyp4f39 WT KO
Elovl1 WT KO
Fatp4 WT KO
nmol/mg tissue
NS NDS NP NSD AS ADS AP ASD BS OS ODS OP OSD EOS EODS EOP EOSD
Total
D
NS
NDS
NP
AS
BS
Cyp4f39 KO
Elovl1 KO
Fatp4 KO
ΔWACL −3 −2 −1 0 1 2 3
B
Cyp4f39
Elovl1
Fatp4
WT
KO
N
A
B
O
EO
C
S
DS
P
SD

Fig. 5


A
Degs2
WT
KO
mRNA levels
4
3
2
1
0
**
Cyp4f39
Elovl1
Fatp4
B
Degs1
WT
KO
mRNA levels
4
3
2
1
0
**
*
Cyp4f39
Elovl1
Fatp4

Supplementary Materials and Methods

Lipid extraction from the epidermis

Each epidermis sample (0.95–1.70 mg) was suspended in a tube containing zirconia beads (SARSTEDT, Nümbrecht, Germany), 450 μL of chloroform/methanol (1:2, v/v), and the following ceramide standards labeled with nine deuterium atoms (d_9): *N*-palmitoyl(d_9)-D-*erythro*-sphingosine (d_9-C16:0 NS, 50 pmol), *N*-palmitoyl(d_9)-dihydrosphingosine (d_9-C16:0 NDS, 100 pmol), *N*-palmitoyl(d_9)-D-*ribo*-phytosphingosine (d_9-C16:0 NP, 12.5 pmol), *N*-palmitoyl(d_9)-6-(*R*)-hydroxysphingosine (d_9-C16:0 NH, 12.5 pmol), *N*-(2'-(*R*)-hydroxypalmitoyl(d_9))-D-*erythro*-sphingosine (d_9-C16:0 AS, 50 pmol), *N*-(2'-(*R*)-hydroxypalmitoyl(d_9))-D-*erythro*-sphinganine (d_9-C16:0 ADS, 12.5 pmol), *N*-(2'-(*R*)-hydroxypalmitoyl(d_9))-D-*ribo*-phytosphingosine (d_9-C16:0 AP, 12.5 pmol), and *N*-(2'-(*R*)-hydroxypalmitoyl(d_9))-6-(*R*)-hydroxysphingosine (d_9-C16:0 AH, 12.5 pmol) (all purchased from Avanti Polar Lipids, Alabaster, AL, USA). The epidermis mixture was homogenized by vigorous mixing using a Micro Smash MS-100 (TOMY Seiko, Tokyo, Japan), and the lysate was recovered. The tube was washed with 450 μL of chloroform/methanol (1:2, v/v) and the resulting wash solution was collected and combined with the lysate. The sample was centrifuged (2,600 × *g* for 5 min at room temperature) to separate it into supernatant and pellet. The pellet was saved for the extraction of protein-bound ceramides and the supernatant containing free ceramides was divided into two 450 μL subsamples for alkaline or non-alkaline treatment. A volume of 36 μL of 4 M potassium hydroxide in methanol was added to the alkaline treatment, or 36 μL of methanol to the non-alkaline treatment; then the sample was incubated for 1 h at 37 °C. The sample was neutralized by adding 12 μL of 12 M formic acid and 36 μL of methanol for the alkaline treatment, or a premixed solution of 12 μL of 12 M

formic acid and 36 μL of 4 M potassium hydroxide for the non-alkaline treatment. After the addition of 300 μL of chloroform and 540 μL of water and vigorous mixing, samples were separated into phases by centrifugation (2,600 × *g* for 3 min at room temperature). The lower, organic phase was recovered and dried. The alkaline-treated samples were used for the measurement of N-type and A-type ceramides, while non-alkaline-treated samples were used for O-type and EO-type ceramides.

Protein-bound ceramides were extracted from each pellet as follows. To remove free lipids, the pellet was washed three times with 1 mL of methanol and then incubated twice at 60 °C with 1 mL of 95% methanol for 2 h. Protein-bound ceramides were extracted from the pellet by incubation for 2 h at 60 °C with 1 mL of 1 M potassium hydroxide in 95 % methanol containing the d_9-labeled ceramide standards (d_9-C16:0 AS, 100 pmol; d_9-C16:0 ADS, 25 pmol; d_9-C16:0 AP, 50 pmol; d_9-C16:0 AH, 50 pmol). The sample was neutralized by adding 1 mL of 1 M acetic acid. After the addition of 1 mL of chloroform and vigorous mixing, the phases were separated by centrifugation (2,600 × *g* for 3 min at room temperature). The resulting lower, organic phase was recovered and dried. Identical extraction procedures were performed on tubes without epidermis as blanks.

Supplementary Figure Legends

Fig. S1. Structures and nomenclature of ceramide classes in mammals. (A) Structures of LCBs and FAs. In mammalian ceramides, there are five types of LCB (dihydrosphingosine [DS], sphingosine [S], phytosphingosine [P], 6-hydroxysphingosine [H], and 4,14-sphingadiene [SD]) and six types of FA (nonhydroxy FA [N], α-hydroxy FA [A], β-hydroxy FA [B], ω-hydroxy FA [O], esterified ω-hydroxy FA [EO], and protein-bound ω-hydroxy FA [P-O]). Chain lengths of N-, A-, or B-type FA moieties are mostly C16–C30 (n = 1–15), and those of O-, EO-, or P-O-type moieties are C30–C36 (n = 15–21). The structures of the two P-O type FAs follow the models proposed by Nemes *et al.* (upper structure) [24] and Takeichi *et al.* (lower structure) [5]. The exact structures of the P-O type FAs are still incompletely understood and both models are plausible. (B) Nomenclature of 30 ceramide classes. Each class is represented by a combination of abbreviations corresponding to its FA and LCB moieties. (C) Structures of NS, EOS, and P-OS. Arrows in the P-OS structures denote the ester bonds sensitive to alkaline hydrolysis, whereby OS ceramides are released. (D) Enzymes involved in the synthesis of acylceramides. The acylceramide synthesis pathway includes the following reactions: production of C30–C36 acyl-CoAs by the FA elongases ELOVL1 (elongation from C20–22 to C26 acyl-CoAs) and ELOVL4 (elongation from C26 to C30–C36 acyl-CoAs), ω-hydroxylation of C30–C36 FAs by the FA ω-hydroxylase CYP4F22 (Cyp4f39 in mice), production of O-type C30–C36 acyl-CoAs by the acyl-CoA synthetase FATP4, synthesis of O-type ceramides by the ceramide synthase CERS3, and production of acylceramides via transacylation of linoleic acid from triacylglycerols to the O-type ceramides by the transacylase PNPLA1.

Fig. S2. FA composition of NS in *Cyp4f39* KO, *Elovl1* KO, and *Fatp4* KO mice. Lipids were extracted from the epidermis of E18.5 *Cyp4f39* KO (n = 3), *Elovl1* KO (n = 3), and *Fatp4* KO (n = 3) mice and their corresponding control WT mice (n = 3 each), and NS ceramides were analyzed via LC-MS/MS. Values presented are means + SD, and statistically significant differences from WT mice are indicated (* $P < 0.05$, ** $P < 0.01$; Student's *t*-test).

Fig. S3. FA composition of NDS in *Cyp4f39* KO, *Elovl1* KO, and *Fatp4* KO mice. Lipids were extracted from the epidermis of E18.5 *Cyp4f39* KO (n = 3), *Elovl1* KO (n = 3), and *Fatp4* KO (n = 3) mice and their corresponding control WT mice (n = 3 each), and NDS ceramides were analyzed via LC-MS/MS. Values presented are means + SD, and statistically significant differences from WT mice are indicated (* $P < 0.05$, ** $P < 0.01$; Student's *t*-test).

Fig. S4. FA compositions of NP in *Cyp4f39* KO, *Elovl1* KO, and *Fatp4* KO mice. Lipids were extracted from the epidermis of E18.5 *Cyp4f39* KO (n = 3), *Elovl1* KO (n = 3), and *Fatp4* KO (n = 3) mice and their corresponding control WT mice (n = 3 each), and NP ceramides were analyzed via LC-MS/MS. Values presented are means + SD, and statistically significant differences from WT mice are indicated (* $P < 0.05$, ** $P < 0.01$; Student's *t*-test).

Fig. S5. FA composition of AS in *Cyp4f39* KO, *Elovl1* KO, and *Fatp4* KO mice. Lipids were extracted from the epidermis of E18.5 *Cyp4f39* KO (n = 3), *Elovl1* KO (n = 3), and *Fatp4* KO (n = 3) mice and their corresponding control WT mice (n = 3 each), and AS ceramides were analyzed via LC-MS/MS. Values presented are means + SD, and statistically significant differences from WT mice are indicated (* $P < 0.05$, ** $P < 0.01$; Student's *t*-test).

Fig. S6. FA composition of BS in *Cyp4f39* KO, *Elovl1* KO, and *Fatp4* KO mice. Lipids were extracted from the epidermis of E18.5 *Cyp4f39* KO (n = 3), *Elovl1* KO (n = 3), and *Fatp4* KO (n = 3) mice and their corresponding control WT mice (n = 3 each), and BS ceramides were analyzed via LC-MS/MS. Values presented are means + SD, and statistically significant differences from WT mice are indicated (* $P < 0.05$, ** $P < 0.01$; Student's *t*-test).

Fig. S1

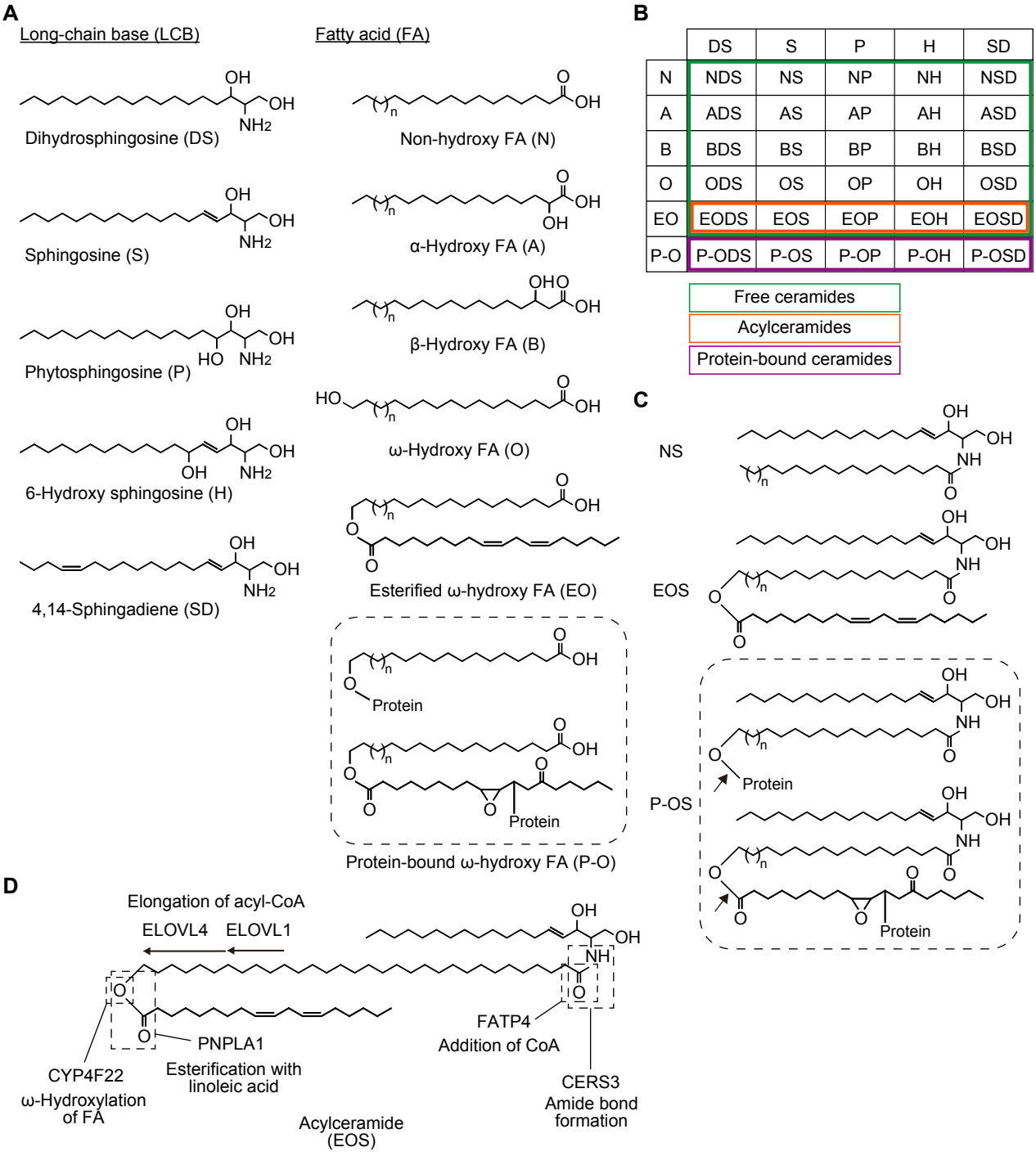

A
Long-chain base (LCB)
Fatty acid (FA)
Dihydrosphingosine (DS)
Sphingosine (S)
Phytosphingosine (P)
6-Hydroxy sphingosine (H)
4,14-Sphingadiene (SD)
Non-hydroxy FA (N)
α-Hydroxy FA (A)
β-Hydroxy FA (B)
ω-Hydroxy FA (O)
Esterified ω-hydroxy FA (EO)
Protein-bound ω-hydroxy FA (P-O)
B
DS S P H SD
N NDS NS NP NH NSD
A ADS AS AP AH ASD
B BDS BS BP BH BSD
O ODS OS OP OH OSD
EO EODS EOS EOP EOH EOSD
P-O P-ODS P-OS P-OP P-OH P-OSD
Free ceramides
Acylceramides
Protein-bound ceramides
C
NS
EOS
P-OS
Protein
D
Elongation of acyl-CoA
ELOVL4 ELOVL1
CYP4F22
ω-Hydroxylation of FA
PNPLA1
Esterification with linoleic acid
FATP4
Addition of CoA
CERS3
Amide bond formation
Acylceramide (EOS)

Fig. S2

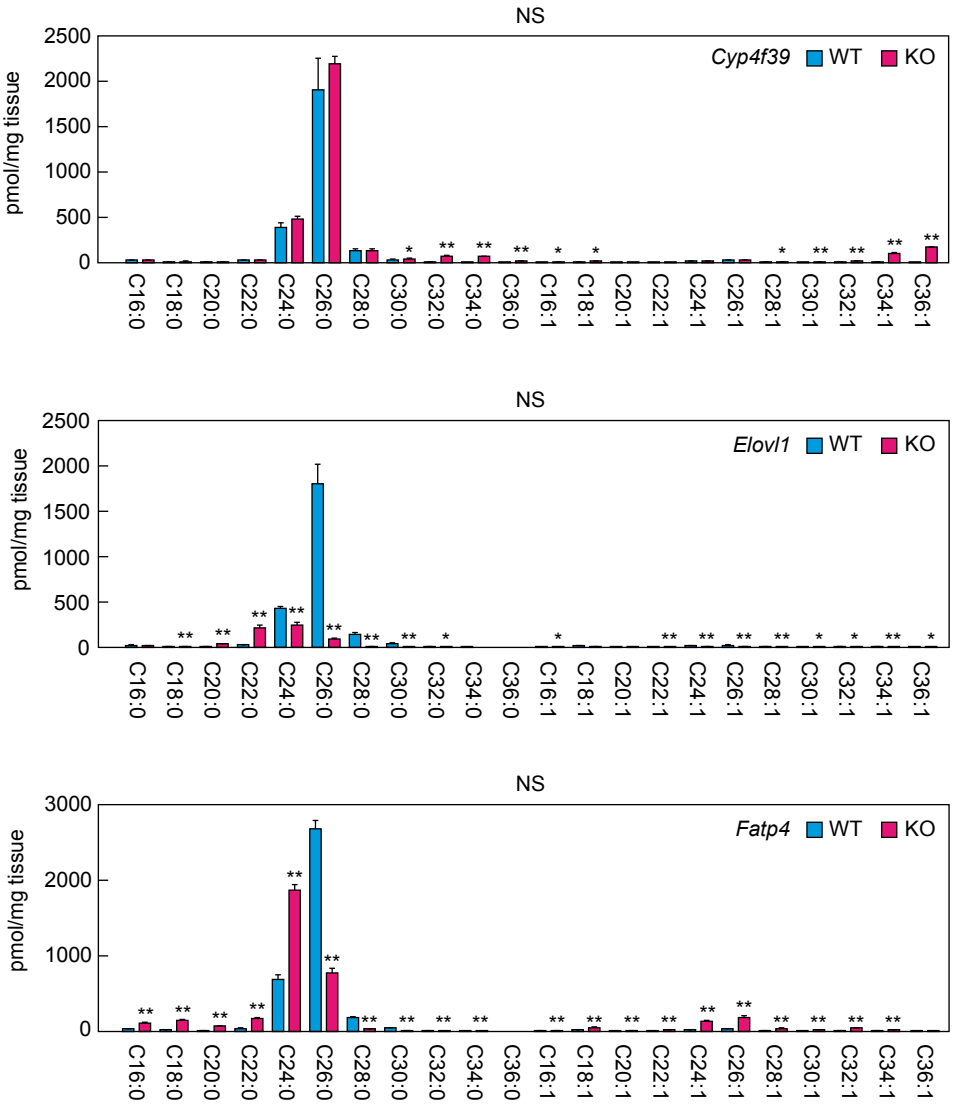

NS
Cyp4f39 WT KO
pmol/mg tissue
2500
2000
1500
1000
500
0
C16:0 C18:0 C20:0 C22:0 C24:0 C26:0 C28:0 C30:0 C32:0 C34:0 C36:0 C16:1 C18:1 C20:1 C22:1 C24:1 C26:1 C28:1 C30:1 C32:1 C34:1 C36:1
NS
Elovl1 WT KO
pmol/mg tissue
2500
2000
1500
1000
500
0
C16:0 C18:0 C20:0 C22:0 C24:0 C26:0 C28:0 C30:0 C32:0 C34:0 C36:0 C16:1 C18:1 C20:1 C22:1 C24:1 C26:1 C28:1 C30:1 C32:1 C34:1 C36:1
NS
Fatp4 WT KO
pmol/mg tissue
3000
2000
1000
0
C16:0 C18:0 C20:0 C22:0 C24:0 C26:0 C28:0 C30:0 C32:0 C34:0 C36:0 C16:1 C18:1 C20:1 C22:1 C24:1 C26:1 C28:1 C30:1 C32:1 C34:1 C36:1

Fig. S3

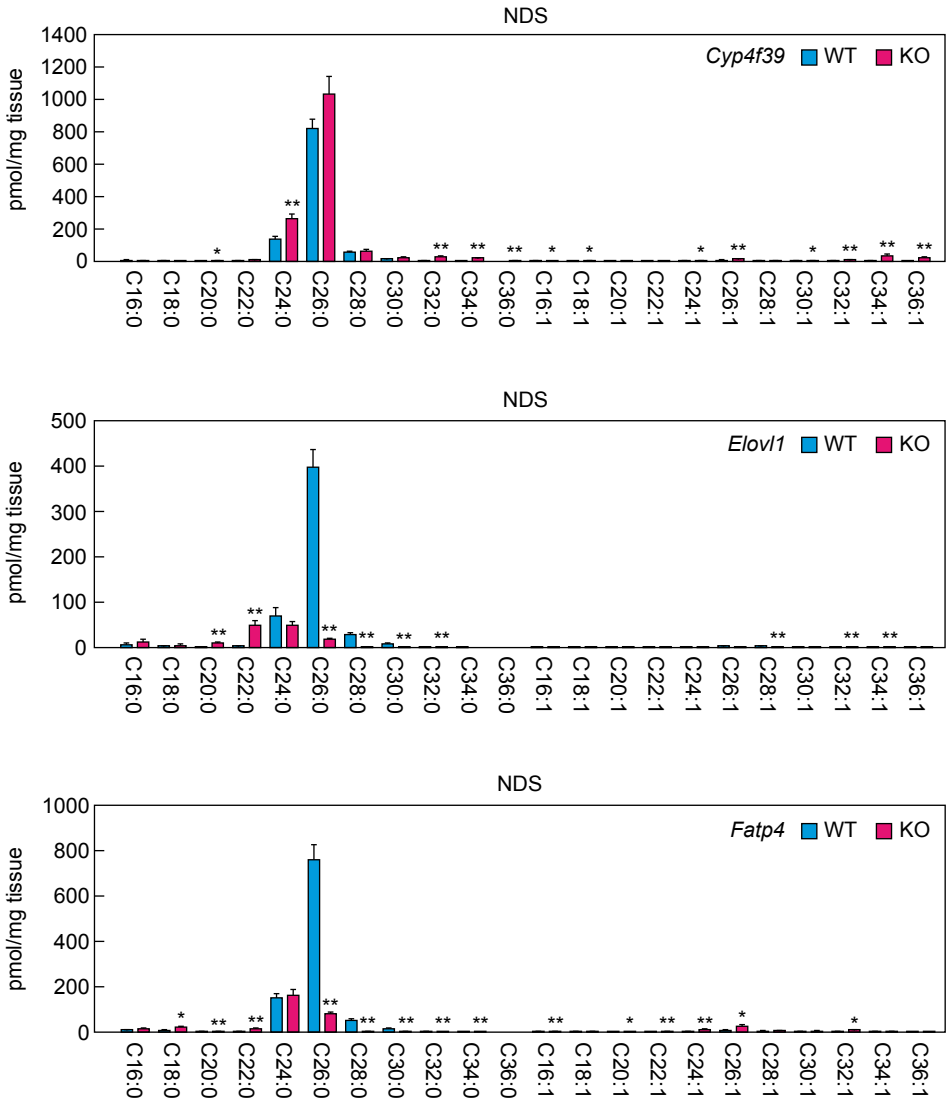

NDS
Cyp4f39 WT KO
pmol/mg tissue
1400
1200
1000
800
600
400
200
0
C16:0 C18:0 C20:0 C22:0 C24:0 C26:0 C28:0 C30:0 C32:0 C34:0 C36:0 C16:1 C18:1 C20:1 C22:1 C24:1 C26:1 C28:1 C30:1 C32:1 C34:1 C36:1
NDS
Elovl1 WT KO
pmol/mg tissue
500
400
300
200
100
0
C16:0 C18:0 C20:0 C22:0 C24:0 C26:0 C28:0 C30:0 C32:0 C34:0 C36:0 C16:1 C18:1 C20:1 C22:1 C24:1 C26:1 C28:1 C30:1 C32:1 C34:1 C36:1
NDS
Fatp4 WT KO
pmol/mg tissue
1000
800
600
400
200
0
C16:0 C18:0 C20:0 C22:0 C24:0 C26:0 C28:0 C30:0 C32:0 C34:0 C36:0 C16:1 C18:1 C20:1 C22:1 C24:1 C26:1 C28:1 C30:1 C32:1 C34:1 C36:1

Fig. S4

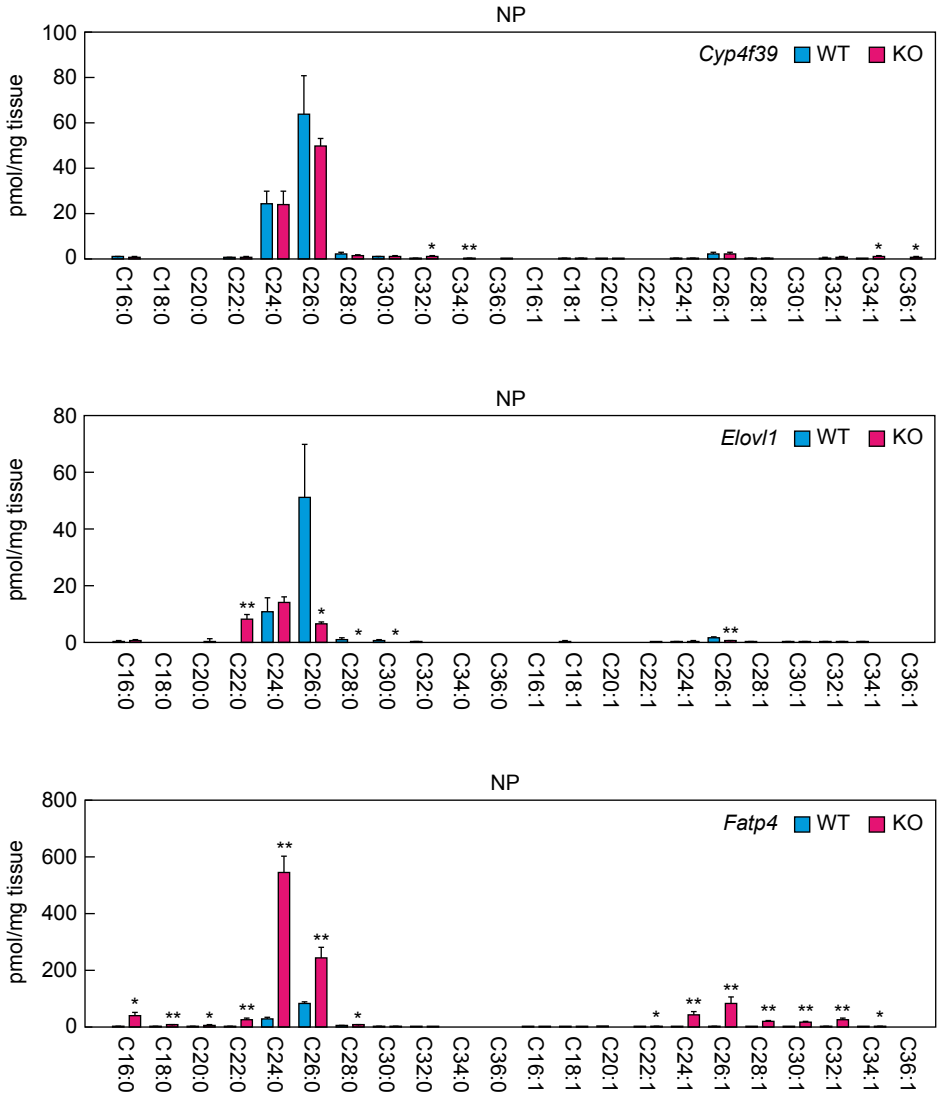

NP
Cyp4f39 WT KO
pmol/mg tissue
0
20
40
60
80
100
C16:0
C18:0
C20:0
C22:0
C24:0
C26:0
C28:0
C30:0
C32:0
C34:0
C36:0
C16:1
C18:1
C20:1
C22:1
C24:1
C26:1
C28:1
C30:1
C32:1
C34:1
C36:1
NP
Elovl1 WT KO
pmol/mg tissue
0
20
40
60
80
NP
Fatp4 WT KO
pmol/mg tissue
0
200
400
600
800

Fig. S5

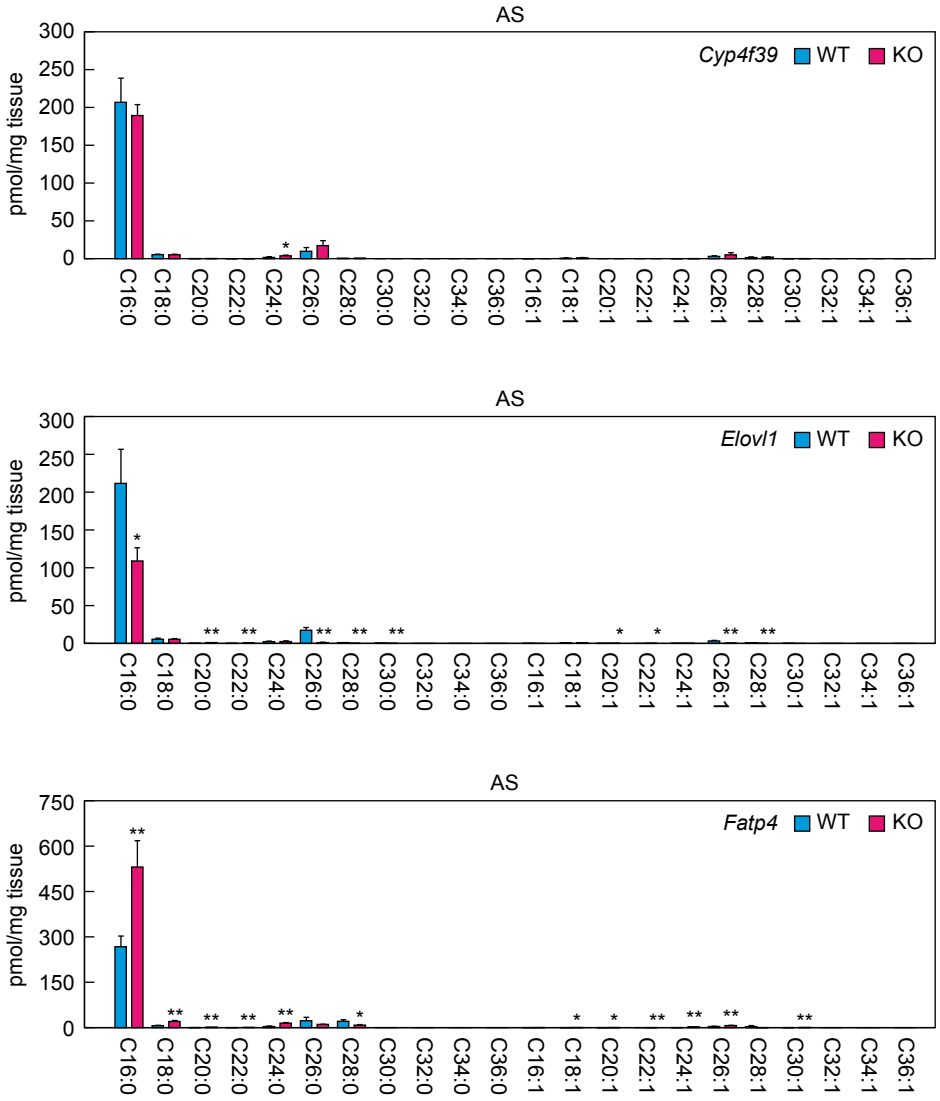
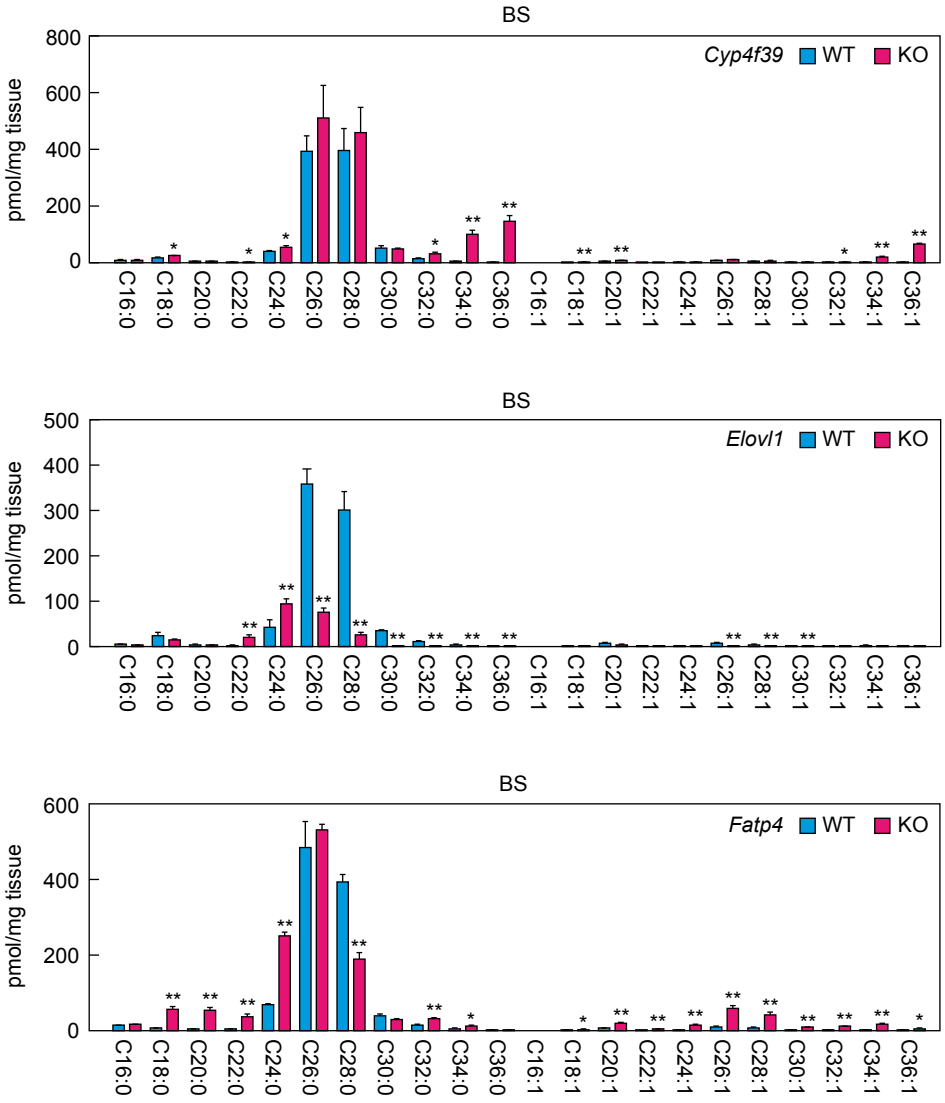

AS
Cyp4f39 WT KO
pmol/mg tissue
300
250
200
150
100
50
0
C16:0 C18:0 C20:0 C22:0 C24:0 C26:0 C28:0 C30:0 C32:0 C34:0 C36:0 C16:1 C18:1 C20:1 C22:1 C24:1 C26:1 C28:1 C30:1 C32:1 C34:1 C36:1
AS
Elovl1 WT KO
pmol/mg tissue
300
250
200
150
100
50
0
C16:0 C18:0 C20:0 C22:0 C24:0 C26:0 C28:0 C30:0 C32:0 C34:0 C36:0 C16:1 C18:1 C20:1 C22:1 C24:1 C26:1 C28:1 C30:1 C32:1 C34:1 C36:1
AS
Fatp4 WT KO
pmol/mg tissue
750
600
450
300
150
0
C16:0 C18:0 C20:0 C22:0 C24:0 C26:0 C28:0 C30:0 C32:0 C34:0 C36:0 C16:1 C18:1 C20:1 C22:1 C24:1 C26:1 C28:1 C30:1 C32:1 C34:1 C36:1

Fig. S6


BS
Cyp4f39 WT KO
pmol/mg tissue
800
600
400
200
0
C16:0 C18:0 C20:0 C22:0 C24:0 C26:0 C28:0 C30:0 C32:0 C34:0 C36:0 C16:1 C18:1 C20:1 C22:1 C24:1 C26:1 C28:1 C30:1 C32:1 C34:1 C36:1
BS
Elovl1 WT KO
pmol/mg tissue
500
400
300
200
100
0
C16:0 C18:0 C20:0 C22:0 C24:0 C26:0 C28:0 C30:0 C32:0 C34:0 C36:0 C16:1 C18:1 C20:1 C22:1 C24:1 C26:1 C28:1 C30:1 C32:1 C34:1 C36:1
BS
Fatp4 WT KO
pmol/mg tissue
600
400
200
0
C16:0 C18:0 C20:0 C22:0 C24:0 C26:0 C28:0 C30:0 C32:0 C34:0 C36:0 C16:1 C18:1 C20:1 C22:1 C24:1 C26:1 C28:1 C30:1 C32:1 C34:1 C36:1